Accepted Manuscript

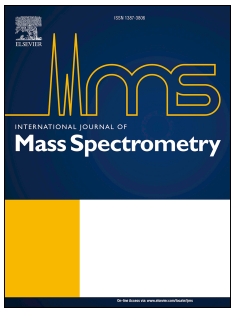

Dueling electrospray implemented on a traveling-wave ion mobility/time-of-flight mass spectrometer: Towards a gas-phase workbench for structural biology

Ian K. Webb, Lindsay J. Morrison, Jeffery Brown

PII: S1387-3806(19)30173-3

DOI: https://doi.org/10.1016/j.ijms.2019.116177

Article Number: 116177

Reference: MASPEC 116177

To appear in: *International Journal of Mass Spectrometry*

Received Date: 24 April 2019

Revised Date: 4 July 2019

Accepted Date: 5 July 2019

Please cite this article as: I.K. Webb, L.J. Morrison, J. Brown, Dueling electrospray implemented on a traveling-wave ion mobility/time-of-flight mass spectrometer: Towards a gas-phase workbench for structural biology, *International Journal of Mass Spectrometry* (2019), doi: https://doi.org/10.1016/j.ijms.2019.116177.

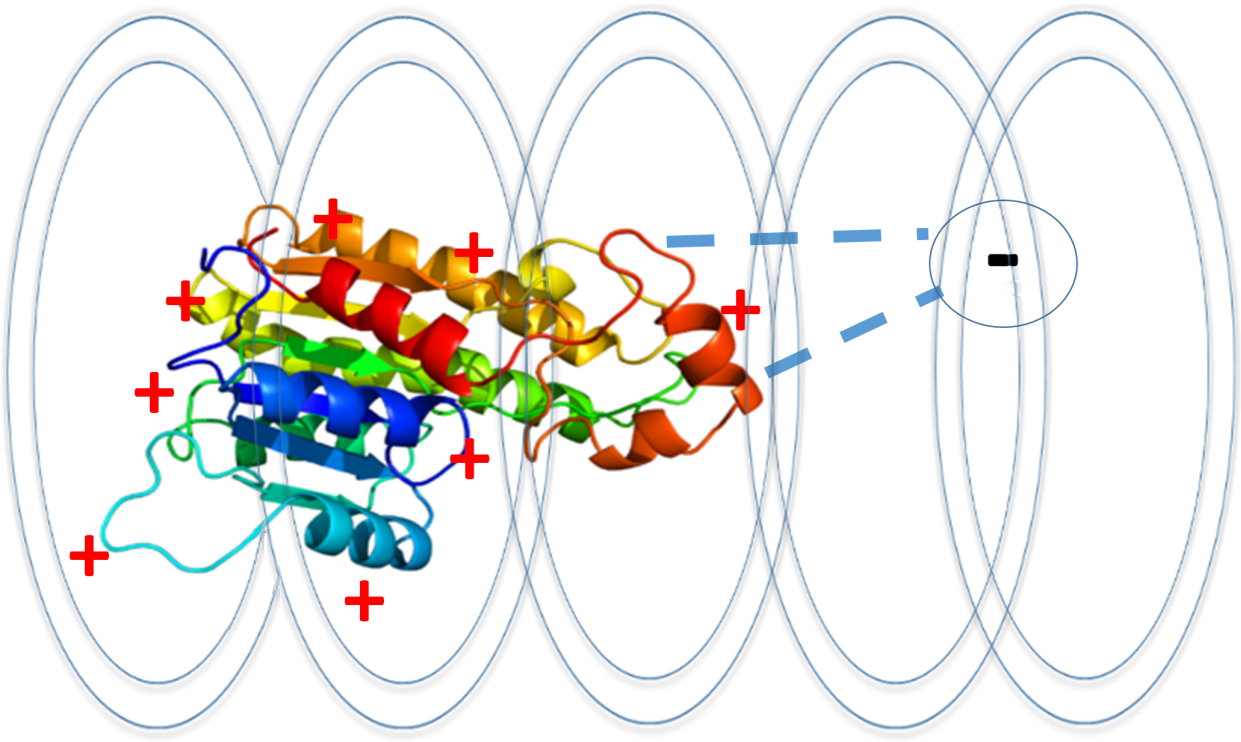

Dueling Electrospray Implemented on a Traveling-Wave Ion Mobility/Time-Of-Flight Mass Spectrometer: Towards a Gas-Phase Workbench for Structural Biology.

Ian K. Webb[1,*], Lindsay J. Morrison[2], Jeffery Brown[3]

[1] Indiana University Purdue University Indianapolis, Indianapolis, IN, USA

[2] Waters Corporation, Beverly, MA, USA

[3] Waters Corporation, Wilmslow, SK9 4AX, UK

[*] Correspondence to Ian K. Webb; e-mail: ikwebb@iu.edu

Keywords: Native mass spectrometry, ion/ion reactions, covalent labeling, ion mobility

Highlights

- Covalent chemistry was performed in an ion mobility/mass spectrometer (IM/MS).
- The effects of various parameters on the extent of reactions was observed.
- Angiotensin I and ubiquitin were covalently labeled in the gas-phase.
- Ion/ion reactions modify ions with solution-like conformations.

Abstract

The traveling wave trap cell of a commercial ion mobility mass spectrometer (IM/MS) was used as a gas-phase reactor for covalent chemistry by making a simple modification to a standard nanoelectrospray source. Reagents and analytes were generated from pulsed opposite polarity nanoelectrospray sources and isolated by their *m/z* prior to reaction. Covalent bond formation was first observed with the model peptide angiotensin I. The modification site was identified as the N-terminus of the peptide by collision induced dissociation (CID). The IM cell separated the covalent reaction product from the proton transfer product by their respective ion mobilities. Next, the effects of several trapping parameters, including the trap traveling wave height, the trap RF voltage, and the trap pressure, were evaluated. Decreasing traveling wave height and increasing RF voltage and pressure increased the number of proton transfer events from apomyoglobin to reagent anions. The 6^+ charge state of ubiquitin generated from nanospray under native-like conditions was covalently modified in the gas phase through ion/ion reactions. Probing the reacted protein with CID led to the assignment of lysine 29 and arginine 54 as reactive nucleophiles accessible to the reagent. IM analysis of the unmodified native-like 6^+ charge state revealed that the gas-phase structure of the protein in the trap was in its compact form. Overall, we introduce a promising method for three-dimensional structural characterization of biomacromolecules.

1. Introduction

Native mass spectrometry (MS) (including tandem MS (MS/MS)), native ion mobility/mass spectrometry (IM/MS), and covalent labeling analyzed by mass spectrometry are widely-used techniques to develop an understanding of how proteins are structured and how their structures relate to their function [1]. Native MS measures masses of intact proteins at high mass accuracy [2-3]. Stoichiometry of intact complexes and subunit masses can be determined by solution- [4-5] or gas-phase [6-7] complex dissociation. IM/MS integrated with native MS also gives the added dimension of protein shape/size. Low-resolution topography maps of entire protein complexes can be generated [8-9].

Covalent labeling analyzed by mass spectrometry illuminates details about protein conformations [10-11] and binding/interacting sites [12-13], determined at the amino acid-residue level. Proteins are modified by covalent labeling strategies in native solution conditions, followed by enzymatic digestion [14]. The identification of modified peptides by liquid chromatography/tandem mass spectrometry (LC/MS/MS) affords the assignment of the location of modification sites. Although this method is not a native mass spectrometry method, covalent labeling has been highly successful in providing native protein structural information.

Though solution-phase covalent labeling gives information about protein folding and binding, protein structures can change between the solution phase and the gas phase. Since IM measures proteins as gas-phase ions, the IM structure may or may not directly correlate to protein structures either in solution or their native environment *in vivo*. Evidence shows that under gentle conditions, the collision cross sections (CCS) from stable, globular proteins can match calculations derived from NMR and X-ray structures [15-16] and FTIR assignments [17].

CCS is a measure of overall ion shape/size, dependent on ion mobility, temperature, buffer gas number density, and the reduced mass for the collision between the ion and buffer gas. However, ion temperatures can increase due to collisional heating if pressures and injection energies are not carefully controlled. The increase in temperature causes smaller proteins and peptides to change conformations [18]. Some non-globular proteins have also been observed to collapse in the gas-phase, giving CCS values smaller than expected from the native structure in solution [19-22]. Additionally, many intact MS methods lack the necessary information to localize folding and protein/protein or small molecule attachment. Thus, uncertainty over the degree to which native structures are maintained in ion mobility experiments remains.

Covalent labeling sample preparation, including labeling, digestion, cleanup, and separation of labeled peptides remains a bottleneck for rapid MS structural characterization. Eliminating this bottleneck is a critical need for taking advantage of the rapid analysis times of MS for structural biology. Covalent labeling does not directly provide the overall size/shape of the protein, and the solution covalent labeling chemistry, enzymatic digestion, and cleanup/separation limit high-throughput analysis. Also, labeling experiments do not characterize gas-phase structures, thereby creating ambiguity between the two techniques with regards to the gas-phase structures measured by IM/MS and the solution structures measured by covalent labeling. Therefore, it is desirable to validate gas-phase structures against solution structures and gain information complementary to size/shape obtainable at much higher speeds than current workflows.

Previous work in gas-phase ion chemistry shows that covalent reactions in the gas-phase are efficient and occur on analytically relevant timescales (i.e., tens of milliseconds) [23-26].

Gas-phase covalent labeling via ion/ion reactions inside of mass spectrometers has been demonstrated for peptides [27-29] and the protein ubiquitin under denaturing conditions [30-31]. These reactions require the presence of an electrostatically "sticky" group to anchor the reagent to the protein to form a long lived complex. The ion/ion reaction method is rapid (mass spectrometer timescale, requires no solution chemistry) but does not directly give the overall structure. Therefore, a technique measuring the overall gas-phase structure (e.g., IM) is needed to complement gas-phase covalent labeling. Here, we demonstrate adaption of an electrospray source for producing opposite polarities of ions to enable covalent labeling reactions in the trap of a commercially available quadrupole/traveling wave IM/time-of-flight (TOF) platform [32]. The IM measurement characterizes the overall shape/size of gas-phase protein ions and gas-phase ion/ion covalent labeling will provide details about the accessibility and reactivity of residue side chains (Figure 1). Herein, we have laid the groundwork for a gas-phase structural biology workbench.

2. Material and Methods

2.1 Materials

Human angiotensin I (DRVYIHPFHL), ubiquitin from bovine erythrocytes, myoglobin from horse heart, ammonium acetate, 2,2,3,3,4,4,5,5,6,6,7,7,8,8,8-pentadecafluoro-1-octanol (PFO), and 4-formylbenzene-1,3-disulfonic acid disodium salt hydrate (FBDSA) were purchased from Sigma-Aldrich (St. Louis, MO). 1-Hydroxy-7-azabenzotriazole (HOAT) was purchased from TCI America (Portland, OR). 1-Ethyl-3-(3-dimethylaminopropyl) carbodiimide hydrochloride (EDC) was purchased from Thermo Scientific (Rockford, IL). Formic acid, acetonitrile, and N, N-dimethyl

formamide (DMF) were purchased from Fisher Scientific (Fairmont, NJ). 3-Sulfobenzoic acid monosodium salt was purchased from Alfa Aesar (Ward Hill, MA). Angiotensin was dissolved in a 50/50/0.1 vol/vol/vol solution of water/acetonitrile/formic acid at 100 nM. FBDSA was used at a 1 µM concentration in 50/50 water/acetonitrile. Myoglobin was prepared at 1 µM in 50/50/0.1 water/acetonitrile/formic acid. Ubiquitin was dissolved in an aqueous 200 mM ammonium acetate solution at 1 µM. 10 mM Sulfo-benzoyl-HOAT was synthesized by a previously published procedure [33] and used at 10 mM in acetonitrile. PFO was dissolved in water/acetonitrile at a concentration of 1 mM of the dimer.

2.2 Instrumentation

All experiments were performed on a Synapt G2-Si HDMS mass spectrometer (Waters Corporation, Wilmslow, U.K.) with electron transfer dissociation (ETD) equipped with the NanoLockspray source with the baffle between the two sprayers removed. The NanoLockspray source contains two nanoelectrospray (nESI) probes, which were used for sequential anion and cation ionization Cations and anions were infused through the sample and reference sprayers, respectively, at flow rates less than 500 nL/min. ETD and mobility modes were used with ETD refill times and intervals of 1 second each. Waters Research Enabled Software (WRENS) was used to apply a 1.5 kV potential to the sample probe during the sample injection phase of the ETD scan function and a -3 kV potential to the reference probe during anion fill. This was accomplished by first decoupling the reference probe from its power supply. Second, the glow discharge voltage source was decoupled from the discharge pin and directly wired to the reference probe. WRENS was also used to ensure proper synchronicity between spray voltages

and instrument lenses. Briefly, the mass spectrometer scan function is as follows: anions were introduced by the reference probe through the stepwave region through the quadrupole, where reagents were isolated by their *m/z* and filled the trap (Figure 2). Next, cations were introduced by the sample probe through the stepwave and specific charge states of interest were isolated by the quadrupole. The potentials in the trap cell were chosen to maintain an excess population of anions in the presence of cations, as the apparent reaction rate of ion/ion reactions is dependent on the number density of reagent ions [34]. Reaction products were gated from the trap for 500 μs into the helium cell by lowering the potential on the exit gate for 500 μs. Next, ions traversed the IM cell filled with N_2 and the transfer cell which contained argon gas. The potential differences between the two sections of the trap, the helium cell, the IM cell, and the transfer cell were tuned to maximize transmission of ion/ion reaction products or increased to effect collision induced dissociation (CID). Ions were mass analyzed by the time-of-flight MS in Resolution Mode (nominal resolving power of 20,000 FWHM). Mobility-selected mass spectra were extracted using the MS data station software (MassLynx V4.2).

3. Results and Discussion

3.1 Implementation of ESI/ESI Ion/Ion Reactions on the Waters Synapt Platform

The Waters Synapt series of instruments is equipped with the ability to perform ETD. This is implemented as follows: the ETD reagent (often a crystalline solid) is placed in a sealed metal container where nitrogen that is swept through the container delivers the neutral reagents to a discharge needle located after the first conductance-limiting orifice of the instrument [25,35]. A discharge voltage is applied to the needle to form gas-phase radical anions of the ETD reagents

by glow-discharge ionization[36-38]. Anions are mass selected by the quadrupole (Figure 2 A) and enter the trap stacked ring ion guide, filled with helium (~0.07 mbar, 18 ml/min helium flow rate). DC biases on the optics are chosen such that potentials become gradually more positive (attractive) to the anions into the trap. During injection of the anion (and cation), there is no traveling wave in the trap. Typically, a repulsive (more negative) DC voltage is applied at the entrance of the helium cell to prevent anions from leaking out of the trap. Next, cations are injected (Figure 2 B). The potentials are switched on the ion optics to provide a negative-going voltage gradient from the source to the trap, drawing cations into the ion trap. A small negative voltage is applied to the entrance of the trap relative to the trap bias in order to prevent anions from leaking out the front of the trap while cations are still filling the trap. After the cation fill, ETD products are gated out of the trap by lowering the trap gate potential (15 V in this case) for a fixed time (500 μs) and by reapplying a traveling wave to the trapping region (typically at traveling wave height <1 V) (Figure 2 C). A voltage diagram showing the conditions for the three states of the experiment (anion fill, cation fill, ion ejection from the trap) is given in Figure 2 D. These events and voltages are all directly controlled from the commercially available version of MassLynx. The ETD products then traverse the helium cell and are separated by their mobilities in the mobility cell, travel through the transfer cell, and are mass analyzed by the time-of-flight. The transfer cell is filled with argon (~0.01 mbar, 1 ml/min argon flow rate) and is divided into two regions which are separately biased. By increasing the bias, the transfer collision energy is increased, allowing for collisional activation and/or CID after ions exit the mobility cell. Thus, CID product ions will have the same drift time as their precursors.

Many capabilities required for covalent ion/ion reactions exist in the commercial implementation of ETD in the Synapt platform. These capabilities include: 1. Isolation reagent and analyte ions by their *m/z*, 2. An RF-confining region to mutually store cations and ions, 3. The ability to form the covalent reaction product by CID prior to the IM cell (i.e., between the trap and He cell regions), 4.) Separation of products from reactants in the mobility cell, and 5.) CID of the mobility-separated products in the transfer cell. Therefore, the voltage diagram shown in Figure 2 D is also used for ESI/ESI ion/ion reactions. The only modification necessary for ESI/ESI reactions was use the second ESI source (the reference probe) to generate anions instead of the glow discharge source. This modification was performed by removing the discharge voltage wire from the discharge pin and attaching it to the reference probe. A simple WRENS script allowed the application of positive and negative ESI voltages to the reference and sample probes synchronized to the anion fill and cation fill, respectively. The discharge voltage source was changed in WRENS from 100 μA mode to 35 μA mode to enable the application of potentials between 0 to -8 kV to the reference probe (in 100 μA mode, only potentials from 0 to -2 kV can be realized). The ETD reagent container was left empty and the nitrogen flow through the container was disabled. No other aspects of the instrument or instrument control were modified.

3.2 Angiotensin 3^+ and FBDSA$^-$

Triply protonated angiotensin I and singly deprotonated FBDSA were reacted in the initial implementation of ESI/ESI ion/ion reactions. This reaction has been directly adapted from previous work on a linear ion trap mass spectrometer [27]. A Schiff base is formed between a

primary amine and aldehyde with water as a leaving group. Long-range coulombic attraction brings the two species together at rates proportional to the square of the charge [34]. The FBDSA reagent is bifunctional, containing both sulfonate and aldehyde functional groups. The high proton affinity of sulfonate results in the stable formation of a long-lived electrostatic complex, with the sulfonate "anchored" to either an ammonium (protonated lysine) or guanidinium (protonated arginine) group [39]. These electrostatic binding strengths have been estimated to be on the order of 28 kcal/mol for binding to protonated lysine and 61 kcal/mol for binding to arginine [40]. Once electrostatically anchored, the main barrier for observing the reaction products is covalent bond formation. Heating the electrostatic complex via energetic collisions will provide a mixture of covalently modified peptides and proton transfer products. The relative sizes of these two fragmentation channels are controlled by the nature of the covalent chemistry and the amount of energy applied to the system. Specifically, the observation of covalent chemistry is maximized if collision energies are chosen above the activation energy for covalent bond formation (less than 20 kcal/mol) but below the activation barrier for proton transfer (i.e. neutral loss of FBDSA) [33,40].

The mass spectrum resulting from the ion/ion reaction of angiotensin 3^+ and FBDSA (Supplemental Figure S1) shows the formation of two products: the charge-reduced angiotensin molecular ion $[M+2H]^{2+}$ and the electrostatically bound complex $[M+3H+FBDSA]^{2+}$. For this experiment, the trap traveling wave voltage was 0.2 V with a wave speed of 300 m/s. Under these conditions, the precursor triply charged angiotensin has been virtually completely reacted away. The formation of covalent products (i.e. neutral loss of water from the electrostatic product) and sequence ions containing the covalent modification are observed in Figure 3A by

increasing the DC bias between the trap cell (0.1 mbar He) and the helium cell (4 mbar He) to 95 V, the helium cell and the IM cell (2.8 mbar N_2) to 50 V, and the IM cell and the transfer cell (0.025 mbar Ar) to 35 V. The ion/ion reaction products and their sequence fragments share identical drift times in their arrival time distributions (ATD) since fragment ions were not formed until after IM separation (Figure 3 B). This is illustrated by Figure 3 C for the covalent modification products. The covalent modification makes the angiotensin cation significantly larger to where it is separated (40 V IM wave height, linear velocity ramp from 900 to 200 m/s) from the proton transfer peak. The mass spectrum with the same drift time as the covalently modified mobility peak shows a typical peptide fragmentation spectrum, with b and y-type ions, with the addition of covalently-modified b_2 and b_3 ions (Figure 3 C). These data alone do not provide evidence whether the modification site is on the N-terminus or the arginine, since the b_1 fragment is not observed, and uncharged arginine is a reactive nucleophile in the gas-phase [29,41]. However, studies with high-energy CID and molecular modeling have revealed that the N-terminus is not protonated in the gas-phase, and that the arginine side chain is protonated [42]. This indicates that Schiff base formation most likely occurs on the N-terminus. An IM separation of ion/ion products prior to their dissociation affords the ability to mass analyze all the fragments in a single experiment while directly linking the fragments to their precursors [43-44]. The combination of IM and CID eliminates the need to perform MS/MS on each of the ion/ion reaction products. Instead, all ion fragmentation can be used, and the fragments will be linked to their precursors. For example, the singly modified angiotensin fragments do not overlap with the doubly modified fragments, as they are separated by the IM

cell. Thus, this method accommodates ion/ion reactions that form multiple products or ion/ion reactions of a complex mixture.

3.3 Characterization of Parameters Affecting Ion/Ion Reactions

The effect of several experimental parameters on glow discharge-based reagents for ion/ion reactions in a traveling wave ion guide has been previously reported [25,35]. We have repeated several of these characterization experiments by proton transfer ion/ion reactions between denatured apomyoglobin cations with PFO dimer anions to characterize ion/ion reactions using the dueling nanoelectrospray source. An excess of at least ten times the ion count of anion to protein was found to be necessary for observing ion/ion reaction products. This is unsurprising due to the linear relationship between the observed reaction rate and the number density of reagent for ion/ion reactions [34]. The parameters found to have the greatest impact on the extent of ion/ion reactions was the trap traveling wave height, the trap RF amplitude, and the helium pressure in the trap. The effects of different traveling wave heights are shown in Figure 4. Figure 4 A shows the reaction of the 16^+ charge state of apomyoglobin with singly deprotonated PFO dimer. Under these conditions, myoglobin transfers up to seven protons, decreasing its charge to the 9^+ charge state, with the center of the charge state distribution at the 13^+ charge state. Increasing the traveling wave amplitude decreases the extent of reaction, with 10+ as the lowest charge state for 0.15 and 0.2 V wave heights (Figure 4 B and C, respectively), and 13+ as the lowest charge state for 0.3 V (Figure 4 D). The base peak of the mass spectrum was 13^+ for 0.1 V, 14^+ for 0.15 V, 15^+ for 0.2 V, and 16+ for 0.3 V. Figure 5 A summarizes these results by weighted average charge state of the distribution (Equation 1).

$$Weighted\ Average\ Charge\ State = \frac{\sum_j^n q_j I_j}{\sum_j^n I_j} \quad (1)$$

Charge states (q) from j to n are multiplied by I, the maximum intensity of each peak and divided by the total intensity of all charge states. The average charge state increases linearly with the traveling wave amplitude from 0.05 to 0.25 V. Above 0.25 volts, the average charge state plateaus. The shape of the curve indicates that the extent of the ion/ion reaction decreases linearly with increasing traveling wave amplitude until the reaction no longer occurs. Decreased traveling wave height results in the improved mixing of cation and anion populations, increasing the number of proton transfer events [25]. The extent of the reaction was also increased by either greatly decreasing (~100 m/s) or increasing (several thousand m/s) the traveling wave speed (data not shown). With the decreased traveling wave speed, in the so-called "surfing condition" when ions move at the speed of the wave, the average ion drift velocities are lower, allowing for more proton transfer events to occur. With greatly increased speed, ions in traveling waves will periodically "roll over" the traveling waves, as their mobilities are too low to allow the ions to remain surfing [25,45-46]. Again, the longer interaction times allow for a greater number of proton transfer events.

Figure 5 B shows the effects of RF amplitude (V_{RF}) on the extent of ion/ion reactions. In this experiment, the extent of the reaction increases between 100 and 500 V_{RF}. The ion cloud density increases with increasing applied V_{RF} [47]. Thus, cations and anions have increased spatial overlap. With better overlap, more proton transfer events occur in the same reaction times. Figure 5 C illustrates the effects of ion trap pressure. The corresponding gas flow rates are indicated in Supplemental Table ST1. There is an increase in the number of proton transfers as the background helium pressure increases, as collisional cooling favors formation of the

ion/ion reaction products [34]. The background pressure becomes too high beyond 0.090 mbar in the trap, reducing signal under the experimental conditions used. As a result of these experiments, the following parameters were used in further studies: 0.1 V trap traveling wave height, 500 V_{RF}, and a pressure of 0.068 mbar (i.e., 18 ml/min trap gas flow rate).

3.4 Interrogating Native Ubiquitin with Ion/Ion Reactions

Ion/ion reactions were applied to native ubiquitin ions in order to assess the three-dimensional structure and relative reactivity of residue side chains in the gas phase. Singly deprotonated sulfo-benzoyl-HOAT was used due to its lower barrier for covalent reaction in the gas phase relative to NHS esters (18 kcal/mol vs. 21 kcal/mol, respectively), with the ability to react with lysine, arginine, histidine, aspartate, and glutamate [31,33]. Figure 6 A shows the ion/ion reaction of ubiquitin 6^+ and sulfo-benzoyl-HOAT$^-$. Several parameters needed to be optimized for efficient covalent bond formation (neutral loss of HOAT from the ion/ion reaction product). Covalent product formation was not favorable at typical gas flows into the helium cell (>100 mL/min). CID in the helium cell was inefficient, and the major product observed was the proton transfer peak $[M+5H]^{5+}$, corresponding to loss of the electrostatically attached reagent. Virtually no covalent bond formation occurred, indicating that too much energy was being added to the system. The most effective way to favorably form covalently-modified products is to apply energy below the threshold for proton transfer product formation over an extended time [40]. However, in the current instrument setup, there is no straightforward way to apply low amplitude collisional “heating” over an extended time period. Therefore, to use lower energies to effect CID and covalent product formation, the gas flows into the helium and IM cells were

lowered to 20 mL/min (0.59 and 0.66 mbar pressures for each of the cells, respectively). This allowed the use of much lower collision energies, with the trapping region of the trap cell at 40 V, the transfer region of the trap cell at 30 V, and the entrance to the helium cell at 10 V relative to the helium cell. The lower collisional energies produced the covalently modified product while resulting in almost no proton transfer. The ATD in Figure 6 B was obtained under these voltage and pressure conditions. The peak at 12 ms corresponds to the unreacted precursor, the peak at ~15 ms corresponds to the addition of one sulfo-benzoyl-HOAT, and the peak at ~19 ms corresponds to the addition of two sulfo-benzoyl-HOAT groups. Figure 6 C shows the mass spectrum at 14.517-15.899 ms, showing covalent bond formation through neutral loss of HOAT. Due to the relatively short time of activation, the electrostatic complex peak was not completely depleted.

The ion/ion reaction results in the addition of up to two sulfo-benzoyl-HOAT reagents to the 6+ charge state. The reaction can proceed further by reducing the cation signal, changing the traveling wave and pressure in the trap cell, and increasing the anion signal. For this study, the trap cell conditions were chosen (300 m/s traveling wave, 0.2 V amplitude, 18 mL/min helium flow into the trap cell) to maximize the intensity of the electrostatic attachment of a single reagent. Next, 45 V of transfer collision energy was applied to perform CID on the covalent reaction product in the transfer cell (1 mL/min argon flow rate, 0.01 mbar) to sequence the modified protein and determine the location of covalent modification.

The identities of the products matching the drift time of the covalently modified precursor were assigned to determine the sites of covalent modification. These were compared to CID of the mass isolated, unreacted 5+ charge state under similar conditions to ensure that

all peaks assigned as covalently modified sequence fragments were only observed in the covalent modification spectrum (Supplemental Figure S2). The results are shown in Figure 7. The smallest unique y ion including the modification was y_{24} (Supplemental Figure S3). The nearest unmodified ion smaller than y_{24} was the unmodified y_{22} ion. Thus, the reaction took place with a side chain between the two cleavage sites. This localizes the modification site to two amino acid residues: glycine 53 and arginine 54. Therefore, one modification site must be arginine 54 since glycine is unreactive towards HOAT ester chemistry. The complementary ion to y_{24}, $b_{52,}$ is also observed as a covalently modified sequence ion. This indicates that there is another side chain with similar surface accessibility and reactivity. The smallest unique modified peptide was b_{32}, and the nearest unmodified neighbor smaller than b_{32} is b_{27}. Thus, the modified residue is between alanine 28 and aspartic acid 32. The observation of the intact covalent modification mass addition in this section of the sequence is best explained by covalent modification of lysine 29.

The sites for covalent modification must be accessible to the reagent and reactive. This precludes buried side chains in the interior of the protein as well as protonated side chains. Recently, 193 nm ultraviolet photodissociation (UVPD) was used to probe the protonation locations of different native charge states of ubiquitin in the gas phase, as UVPD results in fragmentation before protons can mobilize or the protein begins to unfold [48]. The results from the 6+ charge state of ubiquitin are consistent with the ion/ion reaction results and whether the side chains are exposed or buried in the crystal structure (PDB 1UBQ). Neither arginine 54 nor lysine 29 are protonated in the gas phase, and the crystal structure shows that these side chains are on the exterior of the protein, so they are likely candidates for

modification. The only other residue that clearly meets these requirements is lysine 6. Previously, calculated estimates based upon intrinsic gas-phase basicities of the amino acid residues have shown that this lysine has a high gas-phase basicity [49], which indicates that if this residue is unprotonated, it is likely quite reactive toward electrophiles such as the HOAT ester. Future development of an additional gas-phase method to determine protonation sites is warranted to both confirm the results from UVPD and to determine the nature of the lysine 6 residue in the gas-phase.

3.5 Ion Mobility Measurements for Assessing the Structure of Ubiquitin 6^+ in the Trap Cell

Conclusions regarding the applicability of gas-phase protein structural information to solution-phase structures are only meaningful if the gas-phase structure maintains the solution-phase intramolecular and intermolecular interactions. Molecular dynamics simulations using ensembles of solution phase structures for proteins have predicted accurate ion mobility spectra [50]. This method predicts that for a ubiquitin cation with a measured nitrogen CCS reflecting the nitrogen CCS calculated from the X-ray structure of ubiquitin (1209 $Å^2$), solution interactions are maintained. The nitrogen CCS of ubiquitin 6^+ cations were measured under ion/ion reaction conditions but without the introduction of anion to determine the overall structure of the protein in the trap cell. CCS values were measured by calibration with nitrogen literature CCS values and are expected to have a relative error of < 5% [51-52].

IM instruments can cause collisional activation and rearrangement of small proteins like ubiquitin when applying activation energy to drive ions into the mobility cell [18]. Figure 8 shows the effects of increasing injection energy into the mobility cell. Figure 8 A is the ATD of

ubiquitin 6^+ with 30 V of injection energy into the helium cell. The base peak has a measured CCS of 1230 $Å^2$, with a small peak beginning to form at a CCS of 1410 $Å^2$ that is attributed to collisional activation entering the helium cell. Values below 30 V gave no observable signal. No parameters within the chosen range of values of lenses before the trap affected the ATD's appearance, giving evidence that even under the gentlest usable conditions there is some heating when ions are injected into the helium cell, and that the ubiquitin in the trap sampled by ion/ion reactions maintains a native-like structure [15,50]. Increasing the injection energy to 40 V (Figure 8 B) yields a more unfolded distribution, with peaks at 1545, 1790, and 1930 $Å^2$. Figure 8 C shows that with 50 V of injection energy, the distribution is completely extended. Clearly, the ATD is not necessarily indicative of the population in the trap, as in these experiments, only the injection energy into the helium cell (i.e. after ion/ion reactions have taken place) has a major effect on the observed ATD.

. Therefore, though the collisional energy applied after the trap may cause small proteins to unfold, the reaction is indicative of more native-like gas-phase structure. The strong electrostatic binding from the sulfonate group on the reagent to a protonated side chain will anchor the reagent in place when the collision energy to overcome the barrier to covalent reaction is applied. The total through space length of the reagent from the location of covalent bond formation to the sulfonate group is less than 7 Å, which constrains the reaction to nearby amino acid residues. Thus, the side chains that covalently react with the reagent must be within ~10 Å from the anchor site regardless of whether the covalent reaction takes place with native-like or unfolded structures. The reaction is indicative of a limited region on the protein that is reactive to the chemistry. This portion of the polypeptide is accessible and contains a

nucleophilic side chain and charged group with their distance from each other constrained by the size of the reagent. Ubiquitin is a small model protein, and larger proteins and protein complexes, with many more vibrational degrees of freedom and intramolecular and intermolecular interactions, are far less sensitive to collisional unfolding under these conditions, making the energies required for formation of the covalent bond even less likely to unfold structures [53]. Therefore, ion/ion reactions are expected to be an even more effective probe of the structures of larger proteins and protein complexes.

4. Conclusions

We have demonstrated, for the first time, the adaptation of a dual polarity dual electrospray source to a traveling wave IM/MS for ion/ion reactions. We have implemented this method with small peptide and protein models. Ion/ion proton transfer reactions have demonstrated that, unsurprisingly, experimental settings for efficient electron transfer from and proton transfer to radical anions generated by discharge are virtually identical to conditions for efficient ESI/ESI ion/ion reactions. The most important conditions for the reactions were confirmed to be substantial ion cloud overlap in space and in time, low relative velocities, and an excess of reagent ions. The experimental setup is advantageous because it allows for mass selection of reagent anions, ion/ion reactions prior to ion mobility, the ability to collisionally activate ions prior to and after the mobility cell, and fast and high *m/z* range acquisition with the TOF MS. Separating precursors and ion/ion reaction products with IM and multiplexed fragmentation with fragments linked by mobility to their precursors is a distinct advantage for making ion/ion structural measurements.

Ion mobility also provides the overall size/structure of the species being measured by ion/ion reactions. The IM data strongly suggests that we are probing native like conformers of ubiquitin with ion/ion reactions and the location of covalent modifications will be informative of protein native structures in the gas-phase. The covalent modification data pinpoints uncharged, accessible, reactive side chains on the protein, and is consistent with the locations of these side chains in the crystal structure for ubiquitin. Future work is needed for the development of this technology. While CID gave adequate sequence coverage for the small model protein ubiquitin, strategies and methods achieving higher sequence coverage will be necessary for larger proteins. Furthermore, the development of a simple, accurate method for identifying gas-phase protonation sites is warranted to provide additional structural information. Overall, the data presented here shows that this platform is extremely promising for measuring protein structures in the gas phase and, under gentle conditions, a gas-phase method for measuring solution protein structures. We anticipate that this development will also have utility in improving analytical IM separations.

5. Acknowledgement

IKW thanks the IUPUI School of Science and Department of Chemistry and Chemical Biology for research funding.

6. References

[1] Leney, A. C.; Heck, A. J. R., Native Mass Spectrometry: What is in the Name? J. Am. Soc. Mass. Spectrom. 28 (1) (2017) 5-13.
[2] Rose, R. J.; Damoc, E.; Denisov, E.; Makarov, A.; Heck, A. J., High-sensitivity Orbitrap mass analysis of intact macromolecular assemblies. Nat. Methods 9 (11) (2012) 1084-6.
[3] Sharon, M.; Taverner, T.; Ambroggio, X. I.; Deshaies, R. J.; Robinson, C. V., Structural organization of the 19S proteasome lid: Insights from MS of intact complexes. PLoS Biol. 4 (8) (2006) 1314-1323.
[4] Lu, Y.; Goodson, C.; Blankenship, R. E.; Gross, M. L., Primary and Higher Order Structure of the Reaction Center from the Purple Phototrophic Bacterium Blastochloris viridis: A Test for Native Mass Spectrometry. J. Proteome Res. 17 (4) (2018) 1615-1623.
[5] Leary, J. A.; Schenauer, M. R.; Stefanescu, R.; Andaya, A.; Ruotolo, B. T.; Robinson, C. V.; Thalassinos, K.; Scrivens, J. H.; Sokabe, M.; Hershey, J. W. B., Methodology for Measuring Conformation of Solvent-Disrupted Protein Subunits using T-WAVE Ion Mobility MS: An Investigation into Eukaryotic Initiation Factors. J. Am. Soc. Mass. Spectrom. 20 (9) (2009) 1699-1706.
[6] Belov, M. E.; Damoc, E.; Denisov, E.; Compton, P. D.; Horning, S.; Makarov, A. A.; Kelleher, N. L., From Protein Complexes to Subunit Backbone Fragments: A Multi-stage Approach to Native Mass Spectrometry. Anal. Chem. 85 (23) (2013) 11163-11173.
[7] Sahasrabuddhe, A.; Hsia, Y.; Busch, F.; Sheffler, W.; King, N. P.; Baker, D.; Wysocki, V. H., Confirmation of intersubunit connectivity and topology of designed protein complexes by native MS. Proc. Natl. Acad. Sci. U. S. A. 115 (6) (2018) 1268-1273.
[8] Song, Y.; Nelp, M. T.; Bandarian, V.; Wysocki, V. H., Refining the Structural Model of a Heterohexameric Protein Complex: Surface Induced Dissociation and Ion Mobility Provide Key Connectivity and Topology Information. ACS Cent Sci 1 (9) (2015) 477-487.
[9] Loo, J. A.; Berhane, B.; Kaddis, C. S.; Wooding, K. M.; Xie, Y.; Kaufman, S. L.; Chernushevich, I. V., Electrospray ionization mass spectrometry and ion mobility analysis of the 20S proteasome complex. J. Am. Soc. Mass. Spectrom. 16 (7) (2005) 998-1008.
[10] Gau, B. C.; Sharp, J. S.; Rempel, D. L.; Gross, M. L., Fast Photochemical Oxidation of Protein Footprints Faster than Protein Unfolding. Anal. Chem. 81 (16) (2009) 6563-6571.
[11] Vahidi, S.; Stocks, B. B.; Liaghati-Mobarhan, Y.; Konermann, L., Mapping pH-Induced Protein Structural Changes Under Equilibrium Conditions by Pulsed Oxidative Labeling and Mass Spectrometry. Anal. Chem. 84 (21) (2012) 9124-9130.
[12] Liu, T.; Marcinko, T. M.; Kiefer, P. A.; Vachet, R. W., Using Covalent Labeling and Mass Spectrometry To Study Protein Binding Sites of Amyloid Inhibiting Molecules. Anal. Chem. 89 (21) (2017) 11583-11591.
[13] Li, J.; Wei, H.; Krystek, S. R.; Bond, D.; Brender, T. M.; Cohen, D.; Feiner, J.; Hamacher, N.; Harshman, J.; Huang, R. Y. C.; Julien, S. H.; Lin, Z.; Moore, K.; Mueller, L.; Noriega, C.; Sejwal, P.; Sheppard, P.; Stevens, B.; Chen, G.; Tymiak, A. A.; Gross, M. L.; Schneeweis, L. A., Mapping the Energetic Epitope of an Antibody/Interleukin-23 Interaction with Hydrogen/Deuterium Exchange, Fast Photochemical Oxidation of Proteins Mass Spectrometry, and Alanine Shave Mutagenesis. Anal. Chem. 89 (4) (2017) 2250-2258.
[14] Limpikirati, P.; Liu, T.; Vachet, R. W., Covalent labeling-mass spectrometry with non-specific reagents for studying protein structure and interactions. Methods 144 (2018) 79-93.
[15] Wyttenbach, T.; Bowers, M. T., Structural stability from solution to the gas phase: native solution structure of ubiquitin survives analysis in a solvent-free ion mobility-mass spectrometry environment. J. Phys. Chem. B 115 (42) (2011) 12266-75.
[16] Shi, H.; Clemmer, D. E., Evidence for two new solution states of ubiquitin by IMS-MS analysis. J. Phys. Chem. B 118 (13) (2014) 3498-506.

[17] Seo, J.; Hoffmann, W.; Warnke, S.; Bowers, M. T.; Pagel, K.; von Helden, G., Retention of Native Protein Structures in the Absence of Solvent: A Coupled Ion Mobility and Spectroscopic Study. Angew. Chem. Int. Ed. Engl. 55 (45) (2016) 14173-14176.
[18] Merenbloom, S. I.; Flick, T. G.; Williams, E. R., How Hot are Your Ions in TWAVE Ion Mobility Spectrometry? J. Am. Soc. Mass. Spectrom. 23 (3) (2012) 553-562.
[19] Hogan, C. J., Jr.; Ruotolo, B. T.; Robinson, C. V.; Fernandez de la Mora, J., Tandem differential mobility analysis-mass spectrometry reveals partial gas-phase collapse of the GroEL complex. J. Phys. Chem. B 115 (13) (2011) 3614-21.
[20] Devine, P. W. A.; Fisher, H. C.; Calabrese, A. N.; Whelan, F.; Higazi, D. R.; Potts, J. R.; Lowe, D. C.; Radford, S. E.; Ashcroft, A. E., Investigating the Structural Compaction of Biomolecules Upon Transition to the Gas-Phase Using ESI-TWIMS-MS. J. Am. Soc. Mass. Spectrom. 28 (9) (2017) 1855-1862.
[21] Pagel, K.; Natan, E.; Hall, Z.; Fersht, A. R.; Robinson, C. V., Intrinsically Disordered p53 and Its Complexes Populate Compact Conformations in the Gas Phase. Angew. Chem. Int. Ed. 52 (1) (2013) 361-365.
[22] Hansen, K.; Lau, A. M.; Giles, K.; McDonnell, J. M.; Struwe, W. B.; Sutton, B. J.; Politis, A., A Mass-Spectrometry-Based Modelling Workflow for Accurate Prediction of IgG Antibody Conformations in the Gas Phase. Angew. Chem. Int. Ed. 57 (52) (2018) 17194-17199.
[23] McGee, W. M.; McLuckey, S. A., Efficient and directed peptide bond formation in the gas phase via ion/ion reactions. Proc. Natl. Acad. Sci. U. S. A. 111 (4) (2014) 1288-92.
[24] Pilo, A. L.; McLuckey, S. A., Selective Gas-Phase Ion/Ion Reactions: Enabling Disulfide Mapping via Oxidation and Cleavage of Disulfide Bonds in Intermolecularly-Linked Polypeptide Ions. Anal. Chem. 88 (18) (2016) 8972-9.
[25] Lermyte, F.; Verschueren, T.; Brown, J. M.; Williams, J. P.; Valkenborg, D.; Sobott, F., Characterization of top-down ETD in a travelling-wave ion guide. Methods 89 (2015) 22-29.
[26] Laszlo, K. J.; Munger, E. B.; Bush, M. F., Folding of Protein Ions in the Gas Phase after Cation -to-Anion Proton-Transfer Reactions. J. Am. Chem. Soc. 138 (30) (2016) 9581-9588.
[27] Han, H.; McLuckey, S. A., Selective covalent bond formation in polypeptide ions via gas-phase ion/ion reaction chemistry. J. Am. Chem. Soc. 131 (36) (2009) 12884-5.
[28] Mentinova, M.; McLuckey, S. A., Intra- and inter-molecular cross-linking of peptide ions in the gas phase: reagents and conditions. J. Am. Soc. Mass. Spectrom. 22 (5) (2011) 912-21.
[29] McGee, W. M.; Mentinova, M.; McLuckey, S. A., Gas-Phase Conjugation to Arginine Residues in Polypeptide Ions via N-Hydroxysuccinimide Ester-Based Reagent Ions. J. Am. Chem. Soc. 134 (28) (2012) 11412-11414.
[30] Webb, I. K.; Mentinova, M.; McGee, W. M.; McLuckey, S. A., Gas-phase intramolecular protein crosslinking via ion/ion reactions: ubiquitin and a homobifunctional sulfo-NHS ester. J. Am. Soc. Mass. Spectrom. 24 (5) (2013) 733-43.
[31] Pitts-McCoy, A. M.; Harrilal, C. P.; McLuckey, S. A., Gas-Phase Ion/Ion Chemistry as a Probe for the Presence of Carboxylate Groups in Polypeptide Cations. J. Am. Soc. Mass. Spectrom. 30 (2) (2019) 329-338.
[32] Giles, K.; Williams, J. P.; Campuzano, I., Enhancements in travelling wave ion mobility resolution. Rapid Commun. Mass Spectrom. 25 (11) (2011) 1559-66.
[33] Bu, J.; Peng, Z.; Zhao, F.; McLuckey, S. A., Enhanced Reactivity in Nucleophilic Acyl Substitution Ion/Ion Reactions Using Triazole-Ester Reagents. J. Am. Soc. Mass. Spectrom. 28 (7) (2017) 1254-1261.
[34] McLuckey, S. A.; Stephenson, J. L., Ion ion chemistry of high-mass multiply charged ions. Mass Spectrom. Rev. 17 (6) (1998) 369-407.
[35] Laszlo, K. J.; Bush, M. F., Analysis of Native-Like Proteins and Protein Complexes Using Cation to Anion Proton Transfer Reactions (CAPTR). J. Am. Soc. Mass. Spectrom. 26 (12) (2015) 2152-2161.

[36] McLuckey, S. A.; Glish, G. L.; Asano, K. G.; Grant, B. C., Atmospheric sampling glow discharge ionization source for the determination of trace organic compounds in ambient air. Anal. Chem. 60 (20) (1988) 2220-2227.
[37] Reid, G. E.; Mitchell Wells, J.; Badman, E. R.; McLuckey, S. A., Performance of a quadrupole ion trap mass spectrometer adapted for ion/ion reaction studies. Int. J. Mass spectrom. 222 (1) (2003) 243-258.
[38] Earley, L.; Anderson, L. C.; Bai, D. L.; Mullen, C.; Syka, J. E. P.; English, A. M.; Dunyach, J.-J.; Stafford, G. C., Jr.; Shabanowitz, J.; Hunt, D. F.; Compton, P. D., Front-end electron transfer dissociation: a new ionization source. Anal. Chem. 85 (17) (2013) 8385-8390.
[39] Prentice, B. M.; McGee, W. M.; Stutzman, J. R.; McLuckey, S. A., Strategies for the gas phase modification of cationized arginine via ion/ion reactions. Int. J. Mass spectrom. 354 (2013) 211-218.
[40] Bu, J.; Fisher, C. M.; Gilbert, J. D.; Prentice, B. M.; McLuckey, S. A., Selective Covalent Chemistry via Gas-Phase Ion/ion Reactions: An Exploration of the Energy Surfaces Associated with N-Hydroxysuccinimide Ester Reagents and Primary Amines and Guanidine Groups. J. Am. Soc. Mass. Spectrom. 27 (6) (2016) 1089-1098.
[41] Wang, N.; Pilo, A. L.; Zhao, F. F.; Bu, J. X.; McLuckey, S. A., Gas-phase rearrangement reaction of Schiff-base-modified peptide ions. Rapid Commun. Mass Spectrom. 32 (24) (2018) 2166-2173.
[42] Sullards, M. C.; Reiter, J. A., Primary and secondary locations of charge sites in angiotensin II (M+2H)(2+) ions formed by electrospray ionization. J. Am. Soc. Mass. Spectrom. 11 (1) (2000) 40-53.
[43] Hoadlund-Hyzer, C. S.; Li, J. W.; Clemmer, D. E., Mobility labeling for parallel CID of ion mixtures. Anal. Chem. 72 (13) (2000) 2737-2740.
[44] Ibrahim, Y. M.; Prior, D. C.; Baker, E. S.; Smith, R. D.; Belov, M. E., Characterization of an ion mobility-multiplexed collision-induced dissociation-tandem time-of-flight mass spectrometry approach. Int. J. Mass spectrom. 293 (1-3) (2010) 34-44.
[45] Giles, K.; Pringle, S. D.; Worthington, K. R.; Little, D.; Wildgoose, J. L.; Bateman, R. H., Applications of a travelling wave-based radio-frequencyonly stacked ring ion guide. Rapid Commun. Mass Spectrom. 18 (20) (2004) 2401-2414.
[46] Pringle, S. D.; Giles, K.; Wildgoose, J. L.; Williams, J. P.; Slade, S. E.; Thalassinos, K.; Bateman, R. H.; Bowers, M. T.; Scrivens, J. H., An investigation of the mobility separation of some peptide and protein ions using a new hybrid quadrupole/travelling wave IMS/oa-ToF instrument. Int. J. Mass spectrom. 261 (1) (2007) 1-12.
[47] Tolmachev, A. V.; Udseth, H. R.; Smith, R. D., Charge Capacity Limitations of Radio Frequency Ion Guides in Their Use for Improved Ion Accumulation and Trapping in Mass Spectrometry. Anal. Chem. 72 (5) (2000) 970-978.
[48] Morrison, L. J.; Brodbelt, J. S., Charge site assignment in native proteins by ultraviolet photodissociation (UVPD) mass spectrometry. Analyst 141 (1) (2016) 166-176.
[49] Schnier, P. D.; Gross, D. S.; Williams, E. R., On the Maximum Charge-State and Proton-Transfer Reactivity of Peptide and Protein Ions Formed by Electrospray-Ionization. J. Am. Soc. Mass. Spectrom. 6 (11) (1995) 1086-1097.
[50] Bleiholder, C.; Liu, F. C., Structure Relaxation Approximation (SRA) for Elucidation of Protein Structures from Ion Mobility Measurements. J. Phys. Chem. B 123 (13) (2019) 2756-2769.
[51] Sun, Y.; Vahidi, S.; Sowole, M. A.; Konermann, L., Protein Structural Studies by Traveling Wave Ion Mobility Spectrometry: A Critical Look at Electrospray Sources and Calibration Issues. J. Am. Soc. Mass. Spectrom. 27 (1) (2016) 31-40.
[52] Bush, M. F.; Hall, Z.; Giles, K.; Hoyes, J.; Robinson, C. V.; Ruotolo, B. T., Collision Cross Sections of Proteins and Their Complexes: A Calibration Framework and Database for Gas-Phase Structural Biology. Anal. Chem. 82 (22) (2010) 9557-9565.

[53] Eldrid, C.; Ujma, J.; Kalfas, S.; Tomczyk, N.; Giles, K.; Morris, M.; Thalassinos, K., Gas Phase Stability of Protein Ions in a Cyclic Ion Mobility Spectrometry Traveling Wave Device. Anal. Chem. 91 (12) (2019) 7554-7561.

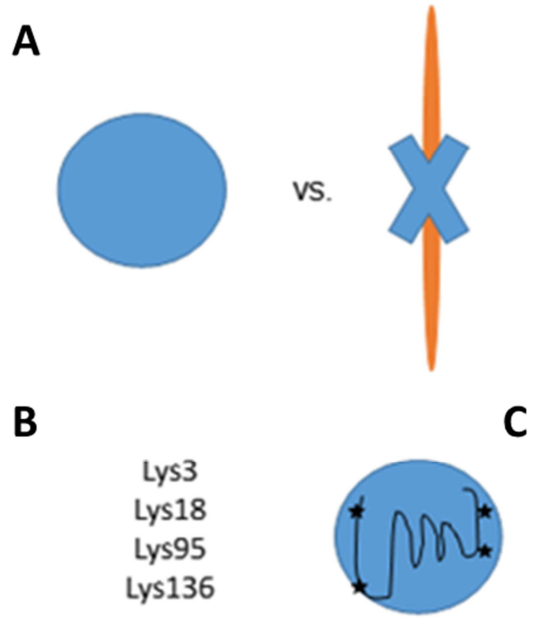

Figure 1. Expected results of ion/ion covalent labeling with IM/MS for a hypothetical protein. **A.** The native CCS measurement reveals that the protein is globular, not linear. **B.** List of hypothetical labeled residues. **C.** Combination of data from the combined approach, where the protein overall shape and size is bounded by the CCS measurement with labeled lysines on the surface of the protein.

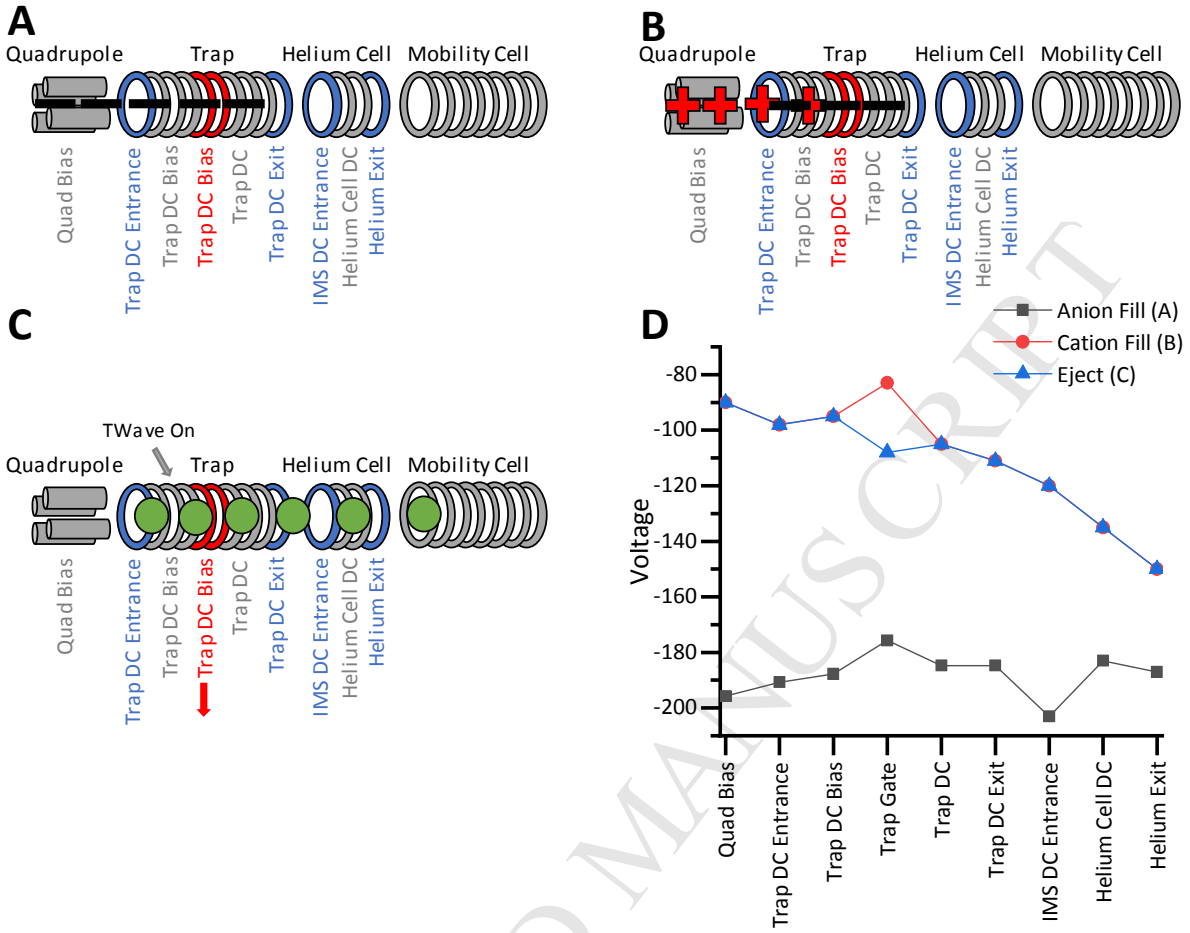

Figure 2. A cartoon of the region of the instrument involved with the ion/ion reactions. The labels below the ion optics correspond to the DC voltages that are applied during the experiment. **A.** Anions (black minus signs) are mass selected in the quadrupole and injected into the trap. **B.** Cations (red plus signs) are isolated and injected to the trap. The trap gate prevents cations from being released. Ion populations overlap and the ion/ion reaction proceeds to products (green circles). **C.** Product ions are pulsed out of the trap with a 500 µs pulse of the trap gate and drift through the ion mobility cell. Products will traverse the transfer cell and into the time-of-flight mass analyzer (not shown). **D.** Voltage diagram for the three states of the trap during the ion/ion reaction.

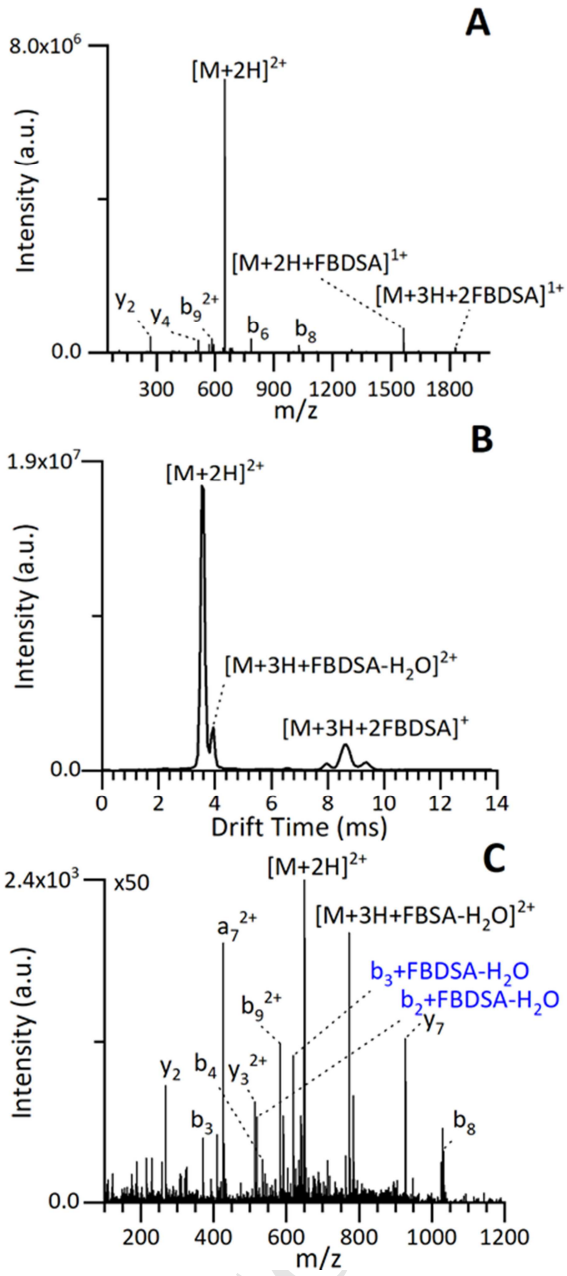

Figure 3. Ion/ion reaction of angiotensin I 3^+ with $FBDSA^-$. **A.** Fragment mass spectrum resulting from CID of the ion/ion reaction products. **B.** ATD corresponding to **A**. **C.** Mass spectrum corresponding to 3.809 to 4.086 ms in the ATD. Covalently modified fragment ions are annotated in blue text. The mass spectrum from the ion/ion reaction prior to CID is reported in Figure S1.

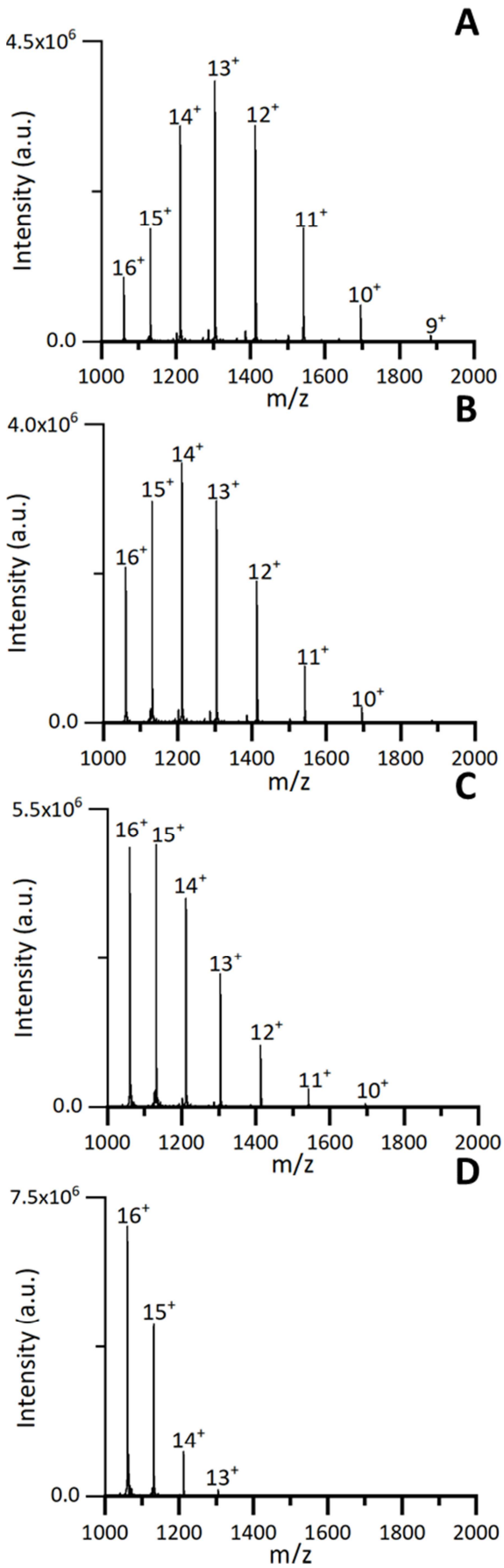
A
4.5x10^6
Intensity (a.u.)
0.0
16+
15+
14+
13+
12+
11+
10+
9+
1000
1200
1400
1600
1800
2000
m/z
B
4.0x10^6
Intensity (a.u.)
0.0
16+
15+
14+
13+
12+
11+
10+
1000
1200
1400
1600
1800
2000
m/z
C
5.5x10^6
Intensity (a.u.)
0.0
16+
15+
14+
13+
12+
11+
10+
1000
1200
1400
1600
1800
2000
m/z
D
7.5x10^6
Intensity (a.u.)
0.0
16+
15+
14+
13+
1000
1200
1400
1600
1800
2000
m/z

Figure 4. Effects of the trap traveling wave voltage on the extent of reaction between apomyoglobin 16^{+} and PFO^{-} dimer. Mass spectra are for traveling wave heights of A. 0.1 V, B. 0.15 V, C. 0.2 V, and D. 0.3 V.

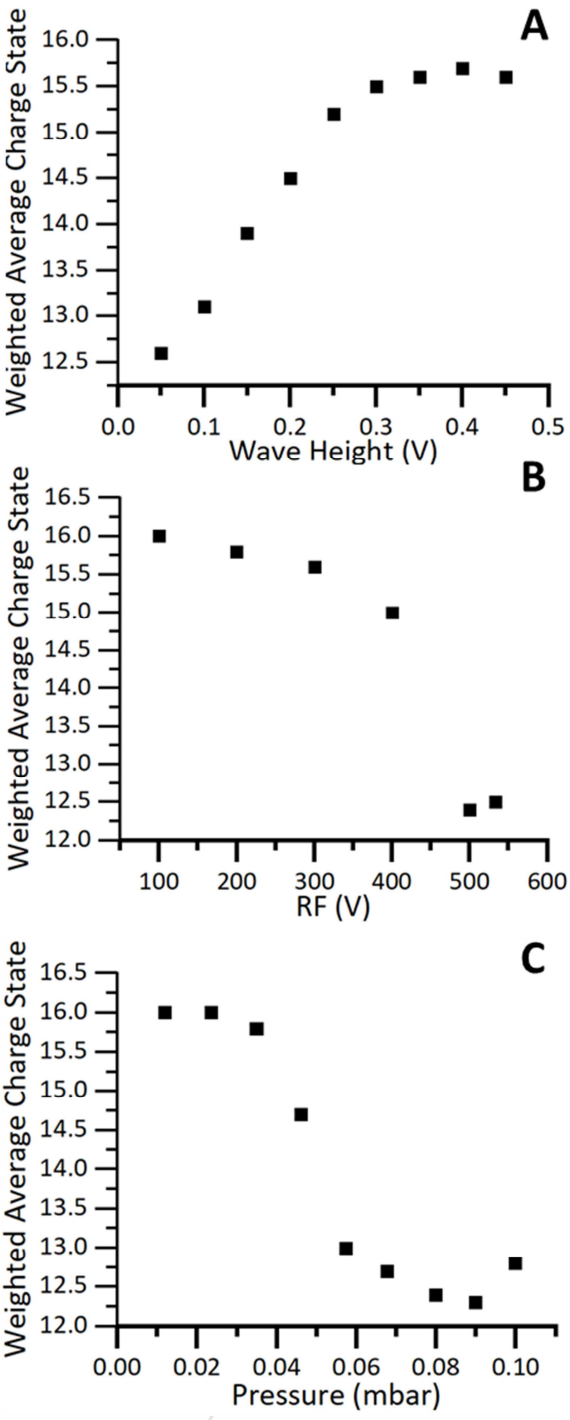

Figure 5. Effects of the **A.** trap traveling wave voltage, **B.** trap RF, and **C.** trap pressure on the extent of reaction between apomyoglobin 16^{+} and PFO^{-} dimer. The extent of the reaction is demonstrated by the weighted average charge state of the charge state distribution.

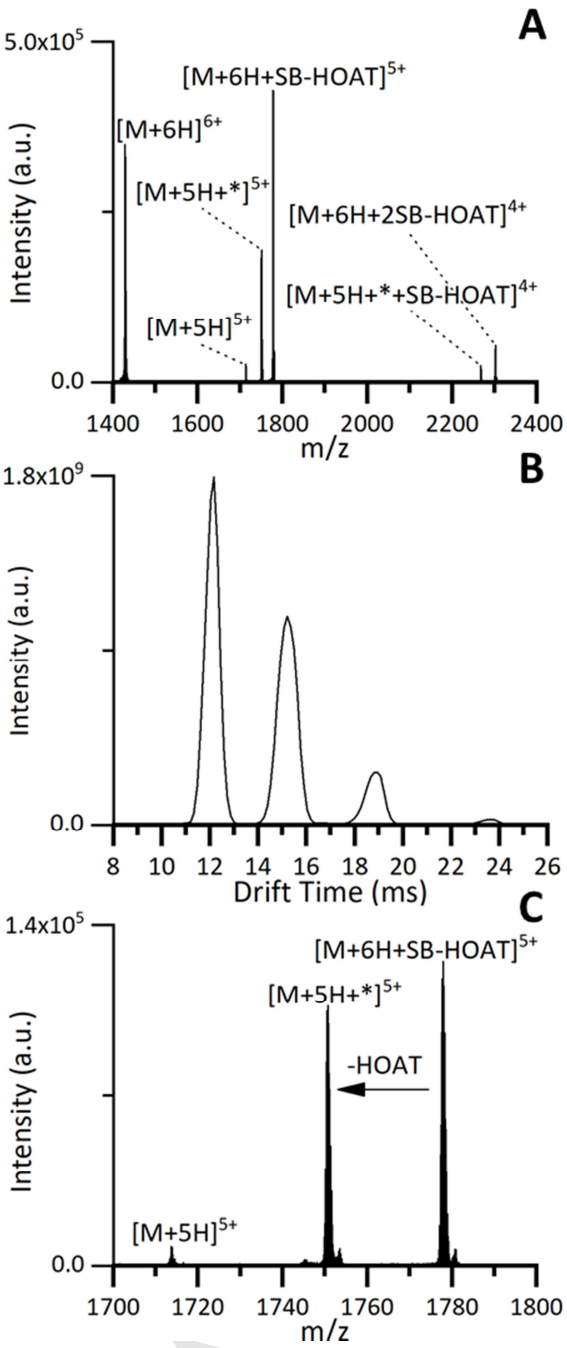

Figure 6. A. Mass spectrum from the ion/ion reaction of ubiquitin 6^+ with sulfo-benzoyl $HOAT^-$ (SB-HOAT). **B.** ATD of ion/ion reaction in **A**. with reduced pressures in the helium cell and IM cell and 40V trap cell bias. **C.** Mass spectrum corresponding to 14.517-15.899 ms in **B**. The * denotes covalent addition of the sulfo-benzoyl moiety through observation of the neutral loss of HOAT.

Figure 7. Sequence ladder of covalently modified ubiquitin 6^{+}. Blue flags indicate fragments that contain the covalent modification. Black flags indicate the largest fragments that have no covalently modified counterpart. The two residues in blue, lysine 29 and arginine 54, are the two sites of covalent modification.

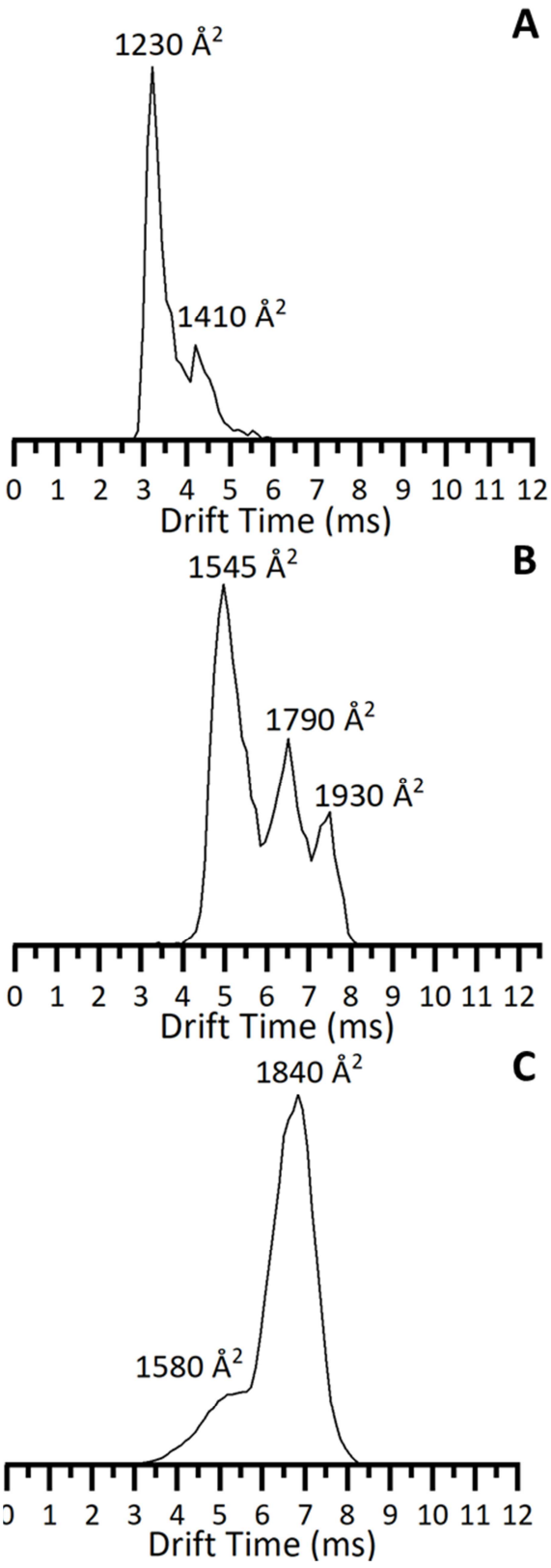

Figure 8. ATD of ubiquitin 6^+ from native conditions with various injection energies. **A.** 30 V, **B.** 40 V, **C.** 50 V.